Aluminum-Induced 1→3-β-D-Glucan Inhibits Cell-to-Cell Trafficking of Molecules through Plasmodesmata. A New Mechanism of Aluminum Toxicity in Plants[1]

Mayandi Sivaguru[2], Toru Fujiwara, Josef Šamaj, František Baluška, Zhenming Yang, Hiroki Osawa, Takanori Maeda, Tomoko Mori, Dieter Volkmann, and Hideaki Matsumoto*

Research Institute for Bioresources, Okayama University, Kurashiki 710–0046, Japan (M.S., Z.Y., H.O., T. Maeda, H.M.); Department of Applied Biological Chemistry, Graduate School of Agricultural and Life Sciences, University of Tokyo, Tokyo 113–8657, Japan (T.F., T. Mori); Precursory Research for Embryonic Science and Technology, Japan Science and Technology Corporation, JST, Chiba 263–1123, Japan (T.F.); Department of Agronomy, Institute of Plant Genetics and Biotechnology, Slovak Academy of Sciences, 950 07 Nitra, Slovakia (J.Š.); Department of Plant Cell Biology, Rheinische Friedrich-Wilhelms-Universität Bonn, D–53115 Bonn, Germany (F.B., D.V.); Bio-Oriented Technology Research Advancement Institution, Omiya 331–8537, Japan (H.O); and Changchun University of Agriculture and Animal Sciences, Changchun, 130062, Peoples Republic of China (Z.Y.)

Symplastic intercellular transport in plants is achieved by plasmodesmata (PD). These cytoplasmic channels are well known to interconnect plant cells to facilitate intercellular movement of water, nutrients, and signaling molecules including hormones. However, it is not known whether Al may affect this cell-to-cell transport process, which is a critical feature for roots as organs of nutrient/water uptake. We have microinjected the dye lucifer yellow carbohydrazide into peripheral root cells of an Al-sensitive wheat (*Triticum aestivum* cv Scout 66) either before or after Al treatment and followed the cell-to-cell dye-coupling through PD. Here we show that the Al-induced root growth inhibition is closely associated with the Al-induced blockage of cell-to-cell dye coupling. Immunofluorescence combined with immuno-electron microscopic techniques using monoclonal antibodies against 1→3-β-D-glucan (callose) revealed circumstantial evidence that Al-induced callose deposition at PD may responsible for this blockage of symplastic transport. Use of 2-deoxy-D-glucose, a callose synthesis inhibitor, allowed us to demonstrate that a reduction in callose particles correlated well with the improved dye-coupling and reduced root growth inhibition. While assessing the tissue specificity of this Al effect, comparable responses were obtained from the dye-coupling pattern in tobacco (*Nicotiana tabacum*) mesophyll cells. Analyses of the Al-induced expression of PD-associated proteins, such as calreticulin and unconventional myosin VIII, showed enhanced fluorescence and co-localizations with callose deposits. These results suggest that Al-signal mediated localized alterations to calcium homeostasis may drive callose formation and PD closure. Our data demonstrate that extracellular Al-induced callose deposition at PD could effectively block symplastic transport and communication in higher plants.

Al is the most abundant metal in the earth's crust, locked up as complex alumino-silicates, which easily release Al^{3+}, a phytotoxic ion, upon soil acidification (Moffat, 1999). In acidic soils, Al is the major constraint for crop production, currently destroying more than 40% of agricultural land around the world (Kochian, 1995). Bringing these lands under cultivation is of prime importance as it has been projected to produce 40% more grain compared with the present day agricultural output to meet the global needs by the year 2020 (Gruhn et al., 1995). Al rapidly inhibits root elongation depending on the Al concentration. Subsequently, this prevents development of the ramified root system, an essential feature for successful plant development (Kochian, 1995). The primary target of Al toxicity is unknown yet, when both apoplastic and symplastic targets are under debate presently (Horst, 1995; Kochian, 1995; Taylor, 1995; Matsumoto, 2000). Nevertheless, available data suggest that Al causes the primary injury in the apoplast of peripheral root cells, where it interferes with essential processes like cell wall assembly, ion fluxes, and plasma membrane (PM) properties (Horst, 1995; Kochian, 1995; Rengel, 1996). However, possible symplastic targets of Al, such as the root cytoskeleton (Barlow and Baluška, 2000), direct binding to nuclei of meristematic root cells (Silva et al., 2000) are not ruled out. Recent reports document

[1] This work was supported by the Program for the Promotion of Basic Research Activities in Innovative Biosciences (PROBRAIN); by the Ministry of Agriculture, Forest and Fisheries, Japan; by a Grant-in-Aid for General Scientific Research (grade A) from the Ministry of Education, Science, Sports and Culture, Japan (to H.M.); by the Ohara Foundation for Agricultural Sciences; by postdoctoral fellowships awarded by the Japan Society for the Promotion of Science (to M.S. and Z.Y.); and by the Alexander von Humboldt Foundation, Germany (to J.Š.).

[2] Present address: Division of Biological Sciences, University of Missouri, 109 Tucker Hall, Columbia, MO 65211–7400.

* Corresponding author; e-mail hmatsumo@rib.okayama-u.ac.jp; fax 81–86–434–1249/1210.

Al-induced alterations to both microtubules and actin cytoskeletal structures, which plays a central role in cell division and elongation (Blancaflor et al., 1998; Seju and Lee, 1998; Sivaguru et al., 1999a, 1999b).

Within a plant cell, the symplast (intracellular space) and apoplast (extracellular space) compartments, although separated via the PM, may not be individual compartments but rather form a functional and structural continuum for exchanging signals and orchestrating development (Wyatt and Carpita, 1993; Miller et al., 1997). The intracellular transport of molecules between plant cells is achieved via minute cytoplasmic channels called plasmodesmata (PD). PD are PM-lined structures traversing cell walls that allow transport of various molecules including small ions, peptides, hormones, and nucleic acids (Ding et al., 1992; Lucas et al., 1993; Lucas, 1995, 1999; Mezitt and Lucas, 1996; Lee et al., 2000). They are also responsible for the spread of viral infection (Lucas and Gilbertson, 1994) and for the formation of developmental and physiological tissue domains (Kragler et al., 1998). Moreover, each PD is equipped with a structurally modified element of endoplasmic reticulum (ER), enriched with calreticulin (Baluška et al., 1999), which interconnects the neighboring cells and provides plant tissues with a membraneous continuity (Baron-Epel et al., 1988).

In animal cells, calcium waves pass through gap junctions, and their openings/closures are rapidly and sensitively modulated via intracellular calcium levels (Sanderson, 1995). Injection of second messenger IP_3 into plant cell, which directly increases the intracellular calcium level through replenishing endocellular calcium stores such as ER, closed PD instantaneously (Tucker, 1988, 1990; Clarke, 1996; Tucker and Boss, 1996). However, after a short period of time once the cytoplasmic calcium levels returned to resting levels, PD re-opened. This suggests that the functional behavior of PD is similar to animal gap junctions. The increase in intracellular calcium is the signal for the activation of 1–3-β-glucan synthase located in PM at PD (Kauss, 1996). Although Al decreases the cytoplasmic calcium levels in suspension-cultured tobacco (*Nicotiana tabacum* L. cv Bright Yellow-2) cells (Jones et al., 1998), it does increase the intracellular calcium levels in cells of intact root hairs (Jones et al., 1999) and wheat (*Triticum aestivum* cv Scout 66) roots (Zhang and Rengel, 1999). This latter event is a prerequisite for the Al-induced callose synthesis (see above). Since the Al-induced callose is initiated as soon as the Al signal is perceived by the cells (Zhang et al., 1994; Horst, 1995 and references therein), one can expect that this may elicit an instantaneous alteration to PD structure and function. By microinjection of fluorescently labeled probe into the root epidermal and cortical cells in the widely studied Al-sensitive wheat (cv Scout 66), we demonstrate that apoplastic Al rapidly induces closure of PD. With the aid of appropriate techniques, we show that the Al-induced callose is likely to be primarily responsible for this PD closure. It is intriguing that increased expression of calcium-binding calreticulin, an ER protein controlling the calcium homeostasis, and unconventional myosin VIII, are closely associated with sites of callose deposition.

RESULTS

Root Growth, Al-Induced Callose Formation, and the Influence of 2-Deoxy-D-Glc

Time-course analysis of root elongation revealed that Al treatment (20 μM, unless stated otherwise) lead to significant growth inhibition from 3 h (Fig. 1A). In the presence of Al, the percentage of root growth over control during the 3-h Al-treatment period was 52%, which was improved prominently (84%) when the roots received 2-deoxy-D-Glc (DDG, 100 μM for 3 h, unless stated otherwise), a specific inhibitor of callose synthesis (Radford et al., 1998) prior to Al treatment (Fig. 1B). DDG treatments alone do not interfere with root growth rates (data not shown). The initial confocal microscopy of semithin (5 μm) sections of root apex after Al treatment re-

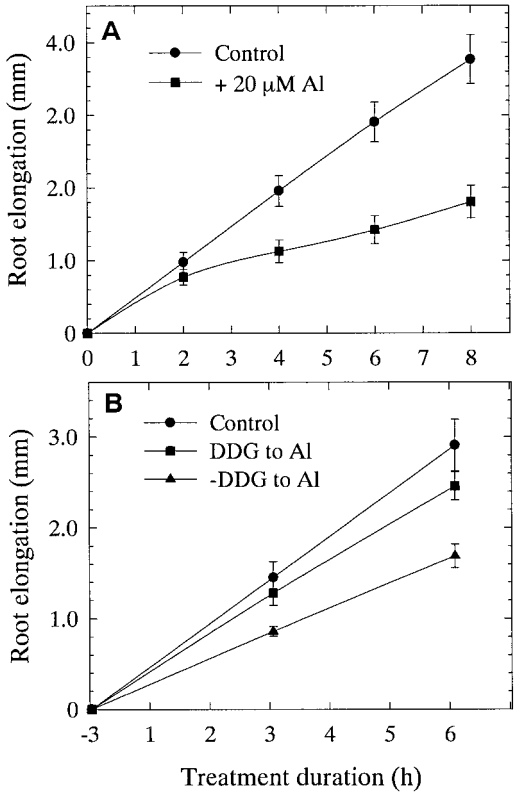

Figure 1. Short-term effects of Al and the influence of DDG (callose synthesis inhibitor) on wheat cv Scout 66 root elongation. Short-term effects of Al (20 μM, up to 8 h) treatment (A) and DDG (100 μM, 3 h) pretreatment followed by Al (6-h) treatment (B). Treatment with DDG (100 μM) alone showed no inhibition during the 9-h growth period (data not shown). Values are means of 10 independent plants ± SE and are representative of at least three independent experiments.

vealed a typical "patchy" pattern of callose accumulation, identical to the one observed by Radford et al. (1998), along the transverse and longitudinal walls of epidermal and cortical cell layers, suggesting their preferential localization to PD regions (Fig. 2, D–F). This patchy pattern of callose was ostensible especially in sections where the cell wall and membraneous regions in the cytoplasmic areas were preserved (paradermal sections). The specificity of dye binding to callose enriched PD/pit field regions was confirmed by the accurate detection of naturally occurring callose from the sieve tube elements of control root PD (Fig. 2C).

To directly test and further confirm the above events of Al-induced callose on PD, we performed immuno-electron microscopy and evaluated callose levels at PD using a monoclonal antibody raised against 1→3 β-D-glucan. In agreement with the confocal images (Fig. 2, E and F), here too the Al-induced callose was localized preferentially at PD regions (Fig. 3). The increase in number of gold particles, especially surrounding PD regions, after Al treatments as well as conspicuous reduction to their number in DDG pretreated roots, all this was apparent with much more enhanced resolution (Fig. 3, B and C). The specificity of antibody binding target sites was also confirmed as the control phloem cells exhibited callose only at sieve tube cell plates (Fig. 3D). The impact of Al on the callose formation at PD and the ameliorative effect of DDG was further substantiated by quantitative evaluation of the immunogold image analysis and by quantitative determination of total callose at 5-mm root apex (Fig. 4). There was approximately more than a 3-fold increase in the number of gold particles localized to the individual PD after Al treatment (Fig. 4A) and approximately a 2-fold reduction to this level if the roots received DDG prior to Al treatment (Fig. 4A). This suggests that DDG can effectively block the Al-induced callose synthesis at PD. The transfer of living roots to fixative for immunogold labeling seemed to induce a transient level of callose within controls, which was also localized preferentially at PD regions (Fig. 3A). A sharp decrease to callose levels in control plants (Fig. 4B) fixed after DDG pre-treatment compared with absolute controls supports this notion. In general, in comparison with the immunogold data the fluorescence spectrophotometric quantification of callose contents, which yielded comparable trends, confirmed both immunogold pattern of callose localization and quantities between treatments (Figs. 3 and 4).

Impact of Al on the Symplastic Cell-to-Cell Trafficking of Molecules through PD

Based on the available reports (see introduction) and from the above experiments, we hypothesized that preferential localization of callose at PD may perturb cell-to-cell communication in cells. Cell-to-cell coupling of the pressure microinjected lucifer yellow carbohydrazide (LYCH), a well-established tool for probing PD gateability (Wolf et al., 1989; Fujiwara et al., 1991), indicated an instantaneous coupling within seconds in epidermal and cortical control cells (Fig. 5, A and A′). The control plants showed approximately a 15% decline in percent dye-coupling (Table I) at a 4- to 5-mm distance from tip (DFT) compared with a 1- to 2-mm DFT. This suggests that cell-to-cell communication as well as the PD frequency is developmentally controlled (see below). Hence, we presume that the impact of any external stimuli is likely to vary along the growth regions of root apex. This presumption is in accordance with data obtained from the intact Arabidopsis roots (Duckett et al., 1994). Since it is well established that the impact of Al varies along specific growth zones of intact root apices (Sivaguru and Horst, 1998; Sivaguru et al., 1999a) and during distinct growth stages of cultured suspension cells (Sivaguru et al., 1999b), the microinjections were performed at both 1- to 2- and 4- to 5-mm DFT regions to assess possible differences of the Al impact (Table I). Apart from a general decline (15%) in the dye coupling in the control, there was no significant differences in percent dye coupling observed between these two DFT regions after Al treatments (Table I). The intact plants pretreated with a range of Al concentrations and treatment durations resulted in apparent decline in cell-to-cell dye coupling at both apical (epidermal, Fig. 5B; and cortex cells, Fig. 5B′) and basal zones (Table I). The percent dye coupling in apical epidermal (Fig. 5C) and cortex cells (Fig. 5C′) was dramatically recovered (several folds) when Al treatments were performed after DDG treatment (Table I). Treatments with DDG alone showed no significant impacts compared with their respective control counter parts. As negative controls, intact root microinjections were performed with 10-kD fluorescein isothiocyanate-dextran, a much larger molecule compared with LYCH (M_r = 453). This resulted in no dye coupling (data not shown), confirming that the cell-to-cell LYCH coupling indeed reflects symplastic transport through the PD.

To test the specificity of this Al-induced closure of PD, microinjections were performed in wild-type tobacco mesophyll leaf cells, an entirely different but widely studied cell/tissue type. Al treatment resulted in significant reductions in the percent of cell-to-cell dye coupling through PD also in tobacco mesophyll cells (Fig. 6, B and B′) compared with controls (Fig. 6, A and A′; Table I).

Having established that whole plant/tissue Al treatment resulted in PD closure, irrespective of the plant tissue type, and since our working hypothesis is that more than 99% Al resides within the apoplast (Horst, 1995; Kochian, 1995; Taylor, 1995; Rengel, 1996; Matsumoto, 2000), next we directly microin-

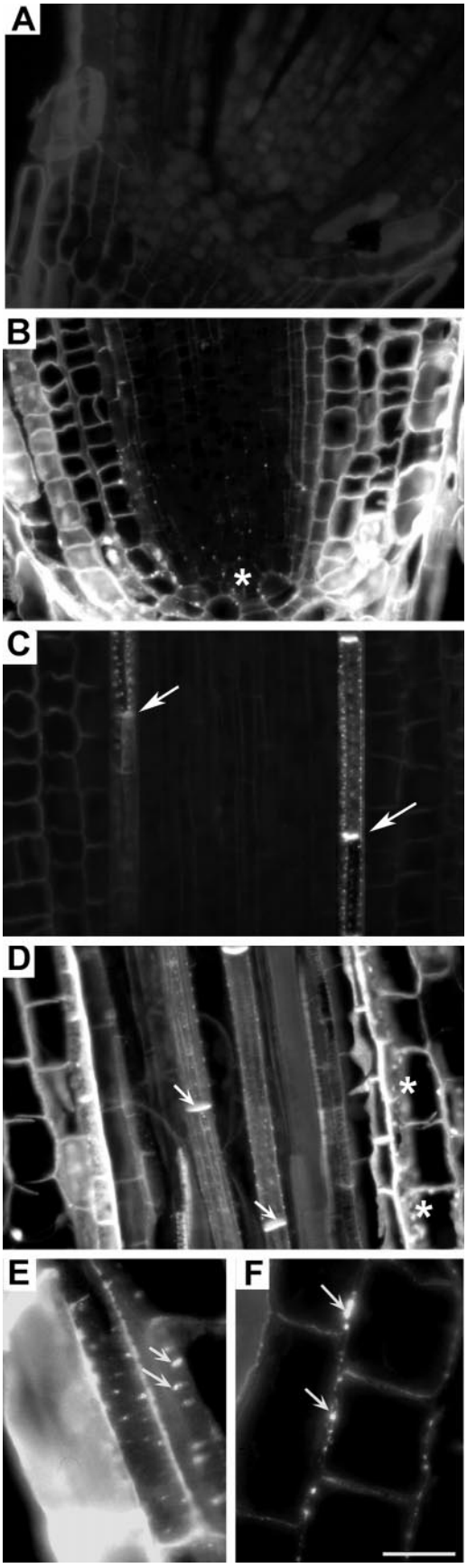

jected Al into the cells to assess possible effects of cytoplasmic Al. These microinjections were performed with a mixture of LYCH and Al (see Table I). It was surprising that, compared with LYCH alone, an instantaneous and more rapid dye coupling was observed in both 3-h Al-pretreated wheat roots (Fig. 7, A–C; Table I) as well as in tobacco mesophyll cells (Fig. 7, D and D′; Table I), indicating a dilating effect of cytoplasmic Al on PD structure and/or function when applied to cytoplasm. This finding suggests that symplastic Al induces PD dilation, which is just the opposite effect on PD response induced by apoplastic Al (preferential localization of Al in apoplast when whole roots are subjected to Al). The novel idea of injecting Al into the cell to study the direct symplastic effects, however, need further detailed analysis by taking Al concentrations, pH, and other cytoplasmic factors into consideration.

Al-Induced Expression and Subcellular Localization of Calreticulin and Myosin VIII

First we tested the specificity of the polyclonal antibodies of calreticulin and myosin VIII in western blots using total root apex (2-mm DFT segments) proteins. Both antibodies showed a high specificity to wheat root calreticulin and myosin VIII (data not shown).

The most prominent feature of calreticulin localization was at the cellular peripheries (Fig. 8). In controls however, the calreticulin fluorescence was at the basal level (Fig. 8A), which increased substantially after Al (20 μM, 3 h) treatments (Fig. 8, B, B′, C, and D) and organized in a patchy pattern (Fig. 8, B and B′). In those cells where the PM, with associated peripheral cytoplasm, was included within a paradermal section through root cells, pit fields of longitudinal walls were characterized with severalfold higher calreticulin fluorescence at both longitudinal and cross walls (Fig. 8, B and B′). In addition, at 1- to 2-mm DFT region, the characteristic higher calreticulin expression at the epidermal/outer cortex junction

Figure 2. Longitudinal thin sections (5 μm) showing Al-induced callose formation in wheat cv Scout 66. Confocal images of aniline blue fluorescence of control (A) and Al-induced (20 μM, 3 h) callose in the root apex (B), in control transition zone stele (C; natural occurrence at the sieve tubes, arrows), in similar region after Al treatments (D; arrows indicate natural sieve tube callose and asterisks indicate Al-induced callose), preferential localization of Al-induced callose at PD/pit-field regions (arrows) in the epidermal (E) and cortical cells (F). Asterisks in B and D indicate callose localization to pit fields. Background is black, and bright white fluorescence indicates callose occurrence. Al-induced patchy pattern of callose at pit-field regions are visible only in paradermal sections (see text for details) or portions of sections (E). Use of confocal microscopy coupled with thin sections revealed the original patchy appearance (from pit-fields) of callose, which is conspicuous mainly at rapidly expanding longitudinal walls compared with radial walls (F). Scale bar represents 25 μm.

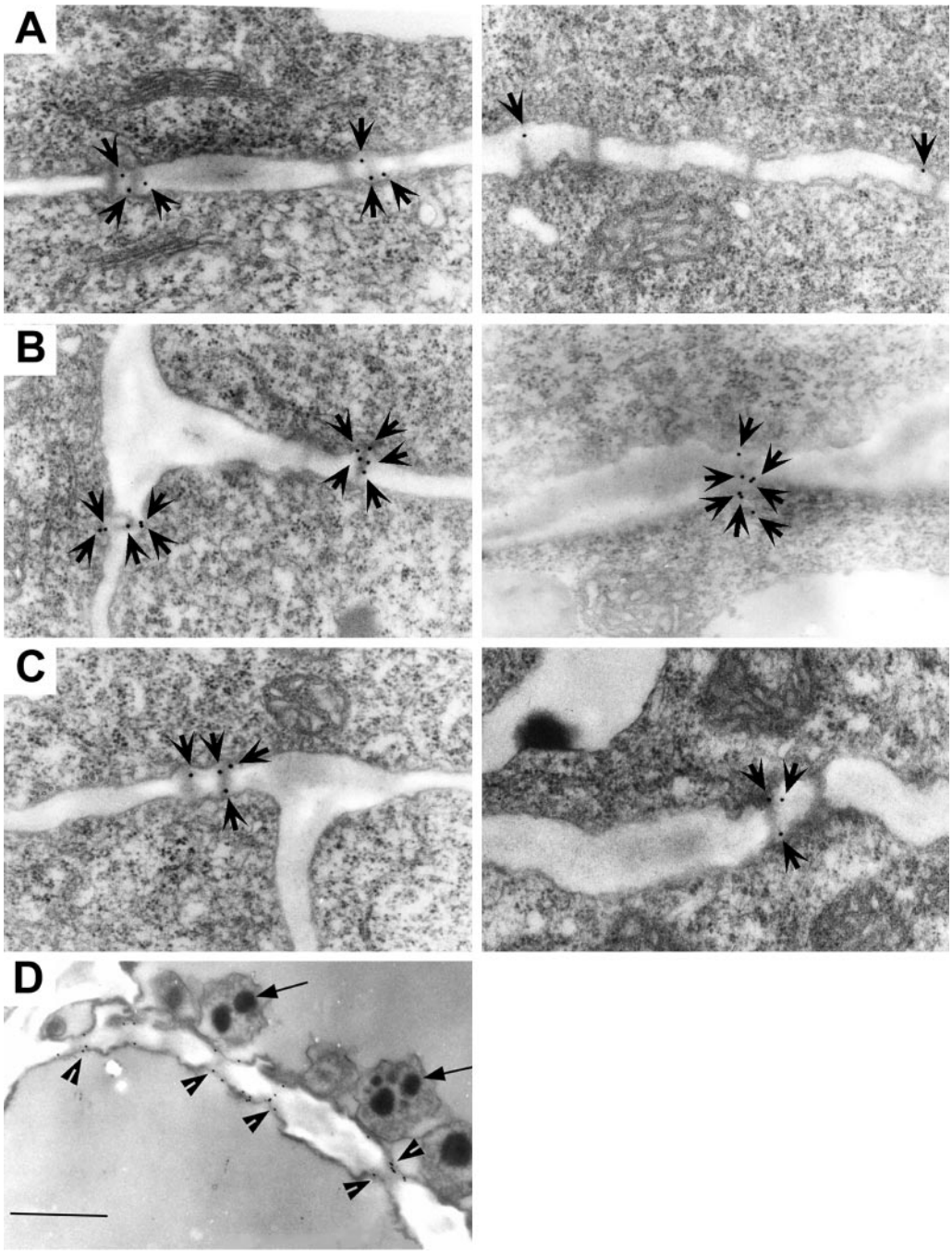

Figure 3. Localization of Al-induced callose in wheat cv Scout 66 using immunogold labeling coupled with transmission electron microscopy. Ultrathin sections of peripheral root cells were incubated with a monoclonal antibody raised against 1→3-β-D-glucan followed by a second antibody conjugated with 15-nm gold particles. All images are from the 1- to 2-mm DFT and show callose particles preferentially at PD regions. Control cells showing few gold particles surrounding PD (A) and increased number of gold particles after Al (3 h, 20 μM) treatments (B), which decreased considerably when the roots received DDG prior to Al treatments (C). Number of arrows correspond to number of gold particles in a single PD (A–C). Representative pair of images from two independent experiments each comprising four to six individual root apices showing similar pattern. D, As a positive control, a single control cell sieve plate showing the antibody specificity. Sieve plates are known to be rich in callose (see also Fig. 2). Sieve cells have P-plastids containing protein crystals (arrows). Note the labeling restricted to defined sieve tubes (arrowheads) and other parts of the cell wall were not labeled. Scale bar represents 0.3 μm.

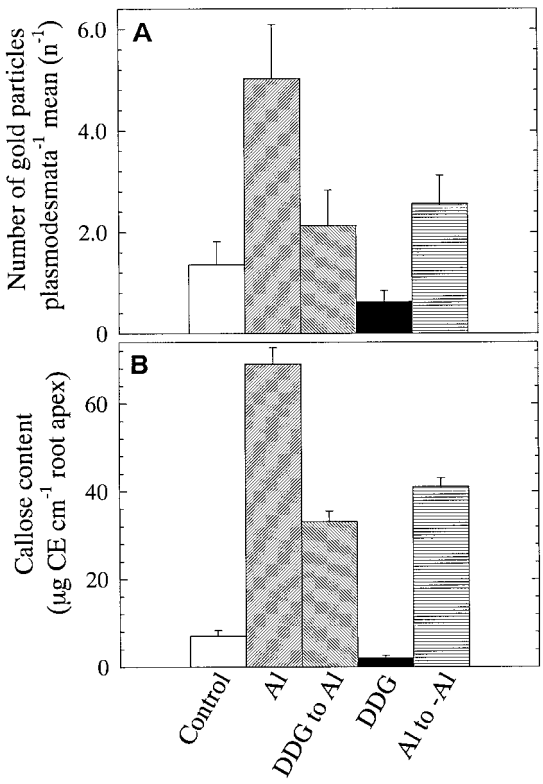

Figure 4. Quantitative evaluation of Al-induced callose formation at PD regions by immunogold labeling (A) and spectrofluorometric quantification of callose (Curdlan equivalents, CE) at the 5-mm root apex (B) of wheat cv Scout 66 plants subjected to a range of indicated treatments. A, Values are number of gold particles counted per individual PD (out of approximately 30–35 PD) alone or organized to pit-fields mean value (average) ± SE. B, Values are mean ± SE of five independent replicates each comprising three 5-mm root segments. While counting gold particles per individual PD especially in control cells, there were some PD, which are weakly labeled and were also included in counting statistics. By contrast, after Al treatments the labeling was much clearer and there were no zero scores. Presented images are representative pattern of at least two independent experiments.

(Fig. 8, C and D) colocalized with the Al-induced callose lining of the PM (Fig. 8, C′ and D′). Because the callose areas here were not paradermal sections (containing cytoplasmic parts, see above), one cannot visualize the patchy appearance of callose here.

Likewise, Al treatments resulted in comparable alterations also with reference to myosin VIII localization (Fig. 9). Myosin VIII localized to the similar PD areas of cell periphery in controls but the intensity was much lesser, except at dividing cells forming new cell walls via callosic cell plates (Figs. 9, A and A′) compared with Al-treated root cells (Fig. 9, B and B′). Especially when the sections encompassed the PM-associated surface (as described above-paradermal sections), an increased myosin VIII expression was evident in Al-treated samples (Fig. 9B′). Between the epidermis and the outer cortex at 1- to 2-mm DFT region, an increased accumulation of myosin VIII (Fig. 9C) co-localized with the Al-induced callose lining of the PM (Fig. 9C′), a feature that was not as prominent as with calreticulin (see above).

DISCUSSION

Our results provide circumstantial evidence that Al-induced callose at the PM-cell wall interface, deposited along the PD sleeve, causes effective blockage of the molecular trafficking and seems to block the intercellular cell-to-cell communication through PD. Compelling evidence is available in literature that PD are not merely static pores in the walls between cells, but that they are gateable channels that have the capacity to dynamically regulate their architecture in response to a variety of external and internal stimuli (Van Bel and Oparka, 1995; Lucas, 1999; Lee et al., 2000). Among such stimuli that prevent the symplastic dye movement or that lead to low frequencies of dye coupling, we can mention turgor pressure gradients (Oparka and Prior, 1992) and exposure of cells to open edges of cut tissues (Van Bel and Oparka, 1995) where callose is deposited. Similar callosic wall apositions are induced in plant cells at sites of fungal contacts (Rodriguez-Gálvez and Mendgen, 1995). All of these suggest that the closure of PD in response to physical stresses and wounding is associated with the formation of additional callose deposits, proposition that was experimentally confirmed using specific inhibitors (Radford et al., 1998). Thus, the gateability of PD seems to be under the control of 1–3-β-glucan synthetase and 1–3-β-D-glucanase activities localized around the PD orifices, driving either synthesis or degradation of callose (Robards and Lucas, 1990; Lucas et al., 1993). In line with these and our present data, Iglesias and Meins (2000) recently demonstrated that enhanced callose depositions at PD of 1–3-β-glucanase deficient mutant delay virus movements due to the reduced PD gateability.

Nevertheless, there must be also other short-term gating mechanisms that are responsible for very rapid and transient closures of PD. These can be induced, for instance, by physiological elevations of cytoplasmic calcium due to transient falls in the temperature and ion injections, revealing that PD can rapidly switch between the "shut-open" modes (Holdaway-Clarke et al., 2000). Such rapid changes in the PD gateability obviously cannot be explained on the basis of callose synthesis/degradation and apparently involve action of calcium-sensitive contractile elements. The size exclusion limit (SEL) of PD differs depending on tissue and cell type (Duckett et al., 1994; Xhu et al., 1998; Gisel et al., 1999; Oparka et al., 1999). Moreover, environmental factors also affect permeability of PD (Gharyal et al., 1989; Epel and Erlanger, 1991). Central issue for understanding these complex phenomena is identification of PD proteins. Several proteins have been immunolocalized to PD pore complex and they are thought to be involved in regulation of the SEL

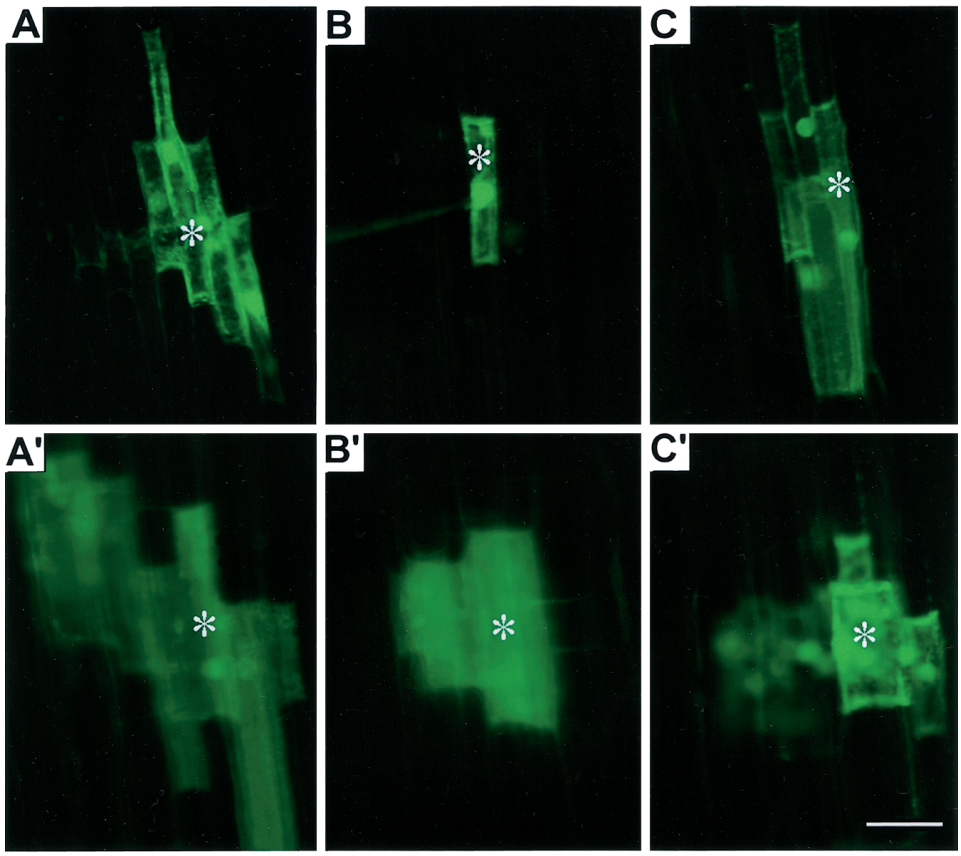

Figure 5. Effect of Al on cell-to-cell trafficking of microinjected fluorescent probe LYCH through PD in wheat cv Scout 66 root apex. Coupling of microinjected LYCH from the injected epidermal (A) and cortex cells (A′) of control roots. Absence of dye coupling in epidermal (B) and a transient coupling in cortex cells (B′) pretreated with Al (3 h, 20 μM). Recovery of dye coupling in epidermal (C) or cortex cells (C′) in plants pretreated with DDG (3 h, 100 μM) prior to Al treatments. Injections were performed in intact plants under optimal conditions and details were provided in "Materials and Methods." Asterisks in all images indicate the injected cell. Presented images are representative of at least three independent experiments. Scale bar represents 15 μm.

selectively, depending on the cellular requirements (Epel, 1994; Lucas, 1995; Zambryski, 1995). Among these PD-associated proteins, we can mention actin (White et al., 1994), myosin-like proteins (Blackman and Overall, 1998; Radford and White, 1998), unconventional myosin VIII (Reichelt et al., 1999), calreticulin (Baluška et al., 1999), calcium-dependent protein kinase (Yahalom et al., 1998), centrin-like protein (Blackman et al., 1999), and viral movement proteins (Epel et al., 1996). While viral movement proteins modifies the PD via increasing the SEL (Lazarowitz and Beachy, 1999), external stimuli, which increases the intracellular calcium levels typically decrease the SEL or close the PD (Tucker, 1990; Holdaway-Clarke et al., 2000). It is interesting that both actomyosin and centrin-like components can perform calcium-dependent contractions.

Intercellular communication via PD is pivotal not only for transport of molecules involved in nutrition but also of signaling molecules including hormones. Especially, the basipetal auxin transport plays a central role in the regulation of root growth (Lomax et al., 1995) and root gravitropism (Rashotte et al., 2000). The recent evidence from Horst group demonstrates that Al effectively inhibits basipetal auxin transport in a root zone-specific manner (Kollmeier et al., 2000). Basipetal auxin flow was Al sensitive especially when Al was applied to the distal part of transition zone (DTZ), which was recently postulated as the Al target of maize root apex (Sivaguru and Horst, 1998; Sivaguru et al., 1999a). When DTZ was treated with Al, simultaneous external auxin supply at central elongation zone alleviated this Al-mediated inhibition of the basipetal auxin transport (Kollmeier et al., 2000). Based on this report, we propose that a potential candidate for this inhibition of auxin signal may be the Al-induced callose, which is severalfold higher in DTZ (Sivaguru and Horst, 1998; Sivaguru et al., 1999a). Also, higher levels of callose accumulation induced by Al in wheat and the circumstantial evidence of its preferential binding to PD (Fig. 3) seems to block the cell-to-cell transport of molecules (Table I). We speculate that the auxin transport carriers (Müller et al., 1998; for review, see Estelle, 1998) may be located at either flanking ends

Table I. *Injection summary showing A1-induced inhibition of cell-to-cell dye (LYCH) coupling through PD in wheat root apex and tobacco mesophyll cells*

Experimental Conditions	Dye Coupling[a]	
	Distance from the tip of the root apex	
	1–2 mm	4–5 mm
Control	13/14 (92.8)	10/13 (76.9)
+A1 (10 μM, 3 h)	7/21 (33.3)	4/16 (25)
+A1 (10 μM, 6 h)	2/12 (16.6)	3/15 (20)
+A1 (20 μM, 3 h)	5/24 (20.8)	2/18 (11.1)
+A1 [(20 μM, 3 h) + (−A1, 3 h)]	5/17 (29.4)	3/19 (15.7)
+DDG (100 μM, 3 h)	9/10 (90.0)	5/5 (100)
+DDG [(100 μM, 3 h) + A1 (20 μM, 3 h)]	14/22 (63.6)	10/21 (47.6)
Injections with A1 (50 nM) + LYCH mixture (v/v)		
Control	11/12 (91.6)	10/11 (90.9)
+A1 (20 μM, 3 h)	16/16 (100.0)	11/12 (91.6)
Tobacco (wild-type) leaf mesophyll cells (*Nicotiana tabacum*)		
Control	8/8 (100.0)	
+A1 (5 μM, 3 h)	2/19 (10.5)	
+A1 (5 μM, 3 h) injection with A1 (50 nM) + LYCH (1 mM) mixture (v/v)	15/16 (93.5)	

[a] Number of successful injections where dye moved from the injected cell/total number of injections. Values in parentheses are the percentage of dye coupling.

of the PD neck region. If this is proven, then activity of these carriers might be physically blocked due to the abundant callose deposition preferentially at PD. Subcellular distribution pattern of auxin transport carriers (Müller et al., 1998) and Al-induced callose (Sivaguru et al., 1999a; Fig. 2, B, E, and F) substantiate this hypothesis. Larsen et al. (1997) proposed that even only when root portions are subjected to Al, there is an Al-specific signal transduction between roots and shoots and presented evidence that exposure of roots to Al rapidly induced callose formation in the shoot apex. Our results of direct Al treatment of tobacco leaf mesophyll cells support this proposal as Al can effectively induce callose in aerial parts of plant cells, which might be the reason for the inhibition of dye coupling (Table I).

Furthermore, Al is well-known to increase the cytoplasmic free calcium levels in root hairs (Jones et al., 1998) and in intact wheat root apices (Zhang and Rengel, 1999), a potential signal inducing new callose synthesis (see introduction). The external stimuli triggering such increases in intracellular-free calcium are known to close higher plant PD (Tucker, 1988, 1990; Clarke, 1996). Moreover, physiological elevations of cytoplasmic calcium levels by cold or other stimuli transiently close PD (Holdaway-Clarke et al., 2000). Our present data on the Al-induced enhanced expression of calcium-binding ER-based calreticulin (Krause and Michalak, 1997), which localize preferentially at PD in root cells (Baluška et al., 1999), suggest that local modifications of PD-based ER element may play a critical part in the Al-induced PD closure. Local alterations in calcium levels may trigger callose formation preferentially at PD. The colocalization of calreticulin and callose after Al treatments strongly support this proposal. In support of this notion, overexpression of calreticulin is closely associated with the increase in intracellular calcium within intracellular stores (Merry et al., 1996). Furthermore, actin cytoskeleton has been suggested to coat the ER in the cytoplasm (Boevink et al., 1998) and apparently accompanies ER elements at and within PD (White et al., 1994; Baluška et al., 2000; Barlow and Baluška, 2000). The actin-associated myosin localized at PD may regulate architecture and gateability of the PD pore complex (Ding et al., 1992, 1996; Overall and Blackman, 1996). Our results clearly indicate that increased expression of calreticulin and myosin VIII under Al exposures both colocalize at callosic pit-fields with Al-induced callose. These data further validate the view that, in addition to Al-induced callose formation, several other events are taking place at the PD pore complex in response to the Al signal, which may finally culminate in the PD closure.

However, rapid cell-to-cell movement of the Al + LYCH in the Al-pretreated root cells indicates that cytoplasmic Al may depolymerize PD-associated actin filaments and microtubules (Blackman and Overall, 1998) and this can dilate the PD pore. For instance, depolymerization of F-actin in tobacco mesophyll cells via cytochalasin D or profilin microinjection has increased the PD permeability (Ding et al., 1996). In support of this proposal, azide-induced anaerobiosis also increased the SEL in wheat roots (Cleland et al., 1994). In line with these findings, we previously demonstrated that Al-induced depolymerization of both F-actin and microtubules (in tobacco suspension cultured cells; Sivaguru et al., 1999b) especially in the Al-sensitive maize root apex (Sivaguru et al., 1999a).

Our data may add a fresh functional tag to the Al-induced callose a very probable primary factor in

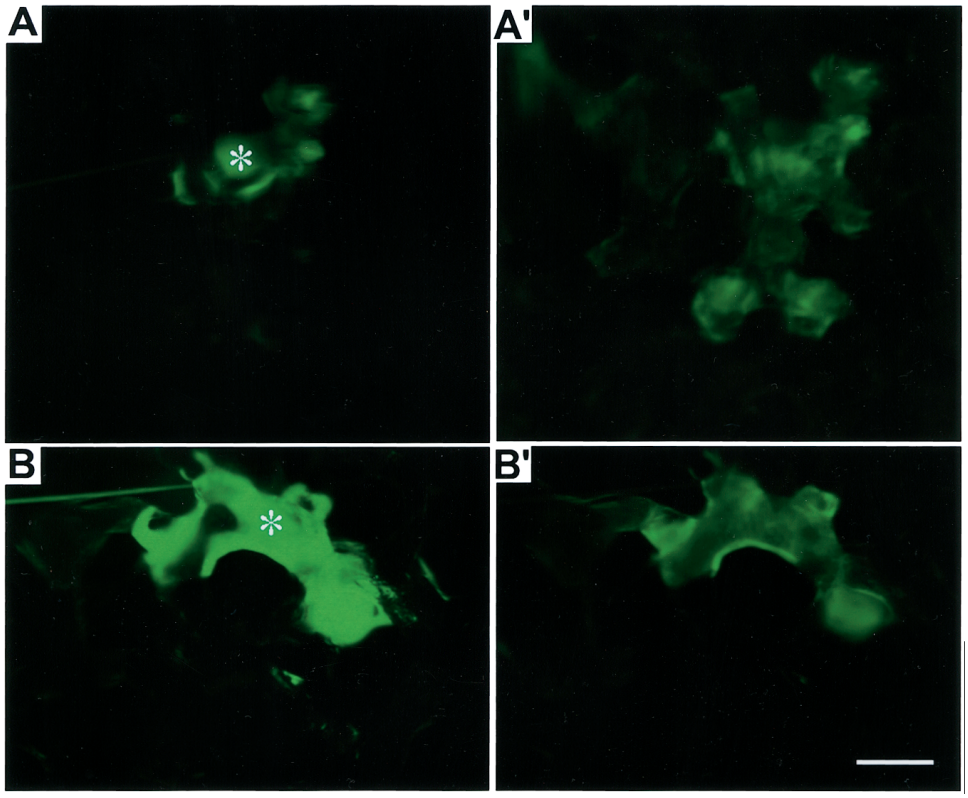

Figure 6. Effect of Al on cell-to-cell trafficking of microinjected fluorescent probe LYCH through PD in wild-type tobacco mesophyll cells. Movement of dye from the injected control cell (A) to neighboring cells (A′). Inhibition of dye coupling was evident, as there was no dye movement from the injected cell (B) and until 3 min (B′) in cells pretreated with Al (5 μM, 3 h). Injections were performed in intact plants under optimal conditions and details were provided in "Materials and Methods." Asterisks in all images indicate the injected cell. Presented images are representative of at least three independent experiments. Scale bar represents 15 μm.

the root growth inhibition by Al. If the symplastic transport is affected by Al-induced callose, one can obviously question what happens to the apoplastic transport during this time. We have measured the Al impact on the apoplastic solute by-pass flow rates in parallel using an Al-sensitive maize with suitable fluorescent marker probes. The results indicate that Al inhibits the apoplastic flow rate significantly, and pretreatment with DDG alleviate this effect moderately and improve it (M. Sivaguru, W.J. Horst, N. Schumol, Z. Yang, H. Matsumoto, unpublished data). In comparison with these results, the present data suggest that Al-induced callose may rapidly block both apoplastic and symplastic transport. This may perturb the indole-3-acetic acid transport along the root apical peripheral cells resulting in the root growth inhibition. Although we cannot rule out the involvement of other factors in the mechanism of Al-toxicity, such as cell wall stiffening and alteration to electrical properties of the PM (Matsumoto, 2000), the present results have both basic and practical implications. They may open an array of avenues for improving the crop performance in acidic-Al soils by understanding more on the PD density, structure, and function in Al-tolerant crop plants. Therefore, our future work will focus on subcellular analysis of Al-induced alterations to localized cytoplasmic calcium levels and diverse cytoskeletal proteins, their inherent relationships with the callose formation at the PM, impact of these factors on the architecture, and gateability of the PD pore complex for a better understanding of the mechanisms behind it.

MATERIALS AND METHODS

Plants, Treatments, and Growth Measurements

Seeds of wheat (*Triticum aestivum* cv Scout 66) were germinated and grown in controlled environmental conditions under 16-/8-h day/night cycles and 25°C constant temperature in hydroponics containing $CaCl_2{\cdot}2H_20$ (0.5 mM, pH 4.5). On d 3, they were transferred to fresh solution of same composition with or without Al (various concentrations of $AlCl_3{\cdot}6H_2O$) for different time periods in well-aerated solutions under several treatment schemes. When necessary, treatment with DDG was carried out for 3 h (100 μM). Seedlings were picked up after designated time point for various analyses. High-sensitivity root growth measurements were performed after marking a 2-cm DFT position with Indian-ink, and elongation was measured by

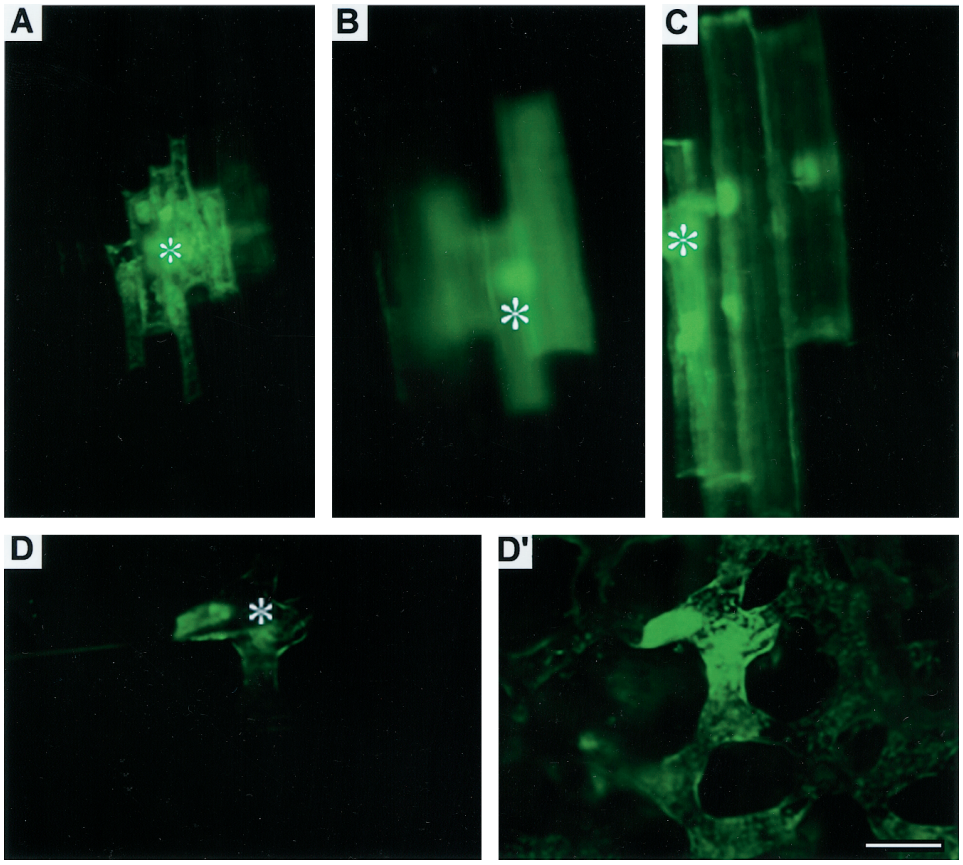

Figure 7. Movement of the microinjected Al and LYCH mixture in Al (20 μM, 3 h) pretreated 1- to 2-mm DFT epidermal (A), cortex (B), and mature 7- to 8-mm DFT region cells (C) of wheat cv Scout 66 root apex. Trafficking of microinjected Al + LYCH mixture in the Al (5 μM, 3 h) pretreated wild-type tobacco mesophyll cells from the injected cell (D) to neighboring cells (D′). Injections were performed in intact plants under optimal conditions and details were provided in "Materials and Methods." Asterisks in all images indicate the injected cell. Presented images are representative of at least three independent experiments. Scale bar represents 15 μm.

recording the movement of the mark under a stereomicroscope (Zeiss-Stemi 2000-C, Zeiss, Oberkochen, Germany) at 20× magnification.

Visual Evaluation of Al-Induced Callose

After treatments, root apices (10 mm) were excised and fixed in 4% (v/v) formaldehyde and processed essentially as described in Sivaguru et al. (1999a). Semithin sections (5 μm) made out of Steedman's wax-embedded material were dewaxed, rehydrated, and then labeled with aniline blue (0.1% [w/v] in Gly/NaOH buffer, pH 9.5), and images were obtained using a confocal microscope (Zeiss-510, Axioplan II, Zeiss) at appropriate excitation and emission wavelengths.

Quantitative Determination of Callose

Callose quantifications were performed essentially as described in Sivaguru and Horst (1998). Briefly, the 96% (v/v) ethanol prefixed roots (5 mm) were washed, blotted dry, and transferred immediately to cups (Eppendorf Scientific, Westbury, NY) containing 1 M NaOH. Callose levels were estimated following the Kauss (1996) method. Each sample containing similarly treated root segments in NaOH was sonicated directly for 1 min. Samples were then placed in a water bath (80°C, 30 min) to solubilize the callose and centrifuged (15 min, 12,000*g*) at room temperature. Callose concentration in the supernatant was quantified fluorometrically at 393-nm excitation and 484-nm emission wavelengths (fluorescence sprectrophotometer, model 4500, Hitachi, Tokyo) using Curdlan as reference.

Immunogold Electron Microscopy

Immunogold labeling of callose was performed essentially as described by Meikle et al. (1991). Briefly, apical 2- to 3-mm-long segments of wheat root tips were excised and fixed in 4% (v/v) formaldehyde in a stabilizing buffer (SB; 50 mM PIPES [1,4-piperazinediethanesulfonic acid], 5 mM EGTA, and 5 mM $MgSO_4$, pH 6.9) for 1.5 h. After thorough washing in SB, root segments were dehydrated in graded ethanol/phosphate-buffered saline (PBS) series and embedded in LR White resin (Hard Grade, British Biocell International, Cardiff, UK), which was allowed to polymerize for 5 d at 36°C in an Al oven in order to preserve the tissue antigenicity. Ultrathin sections obtained using an

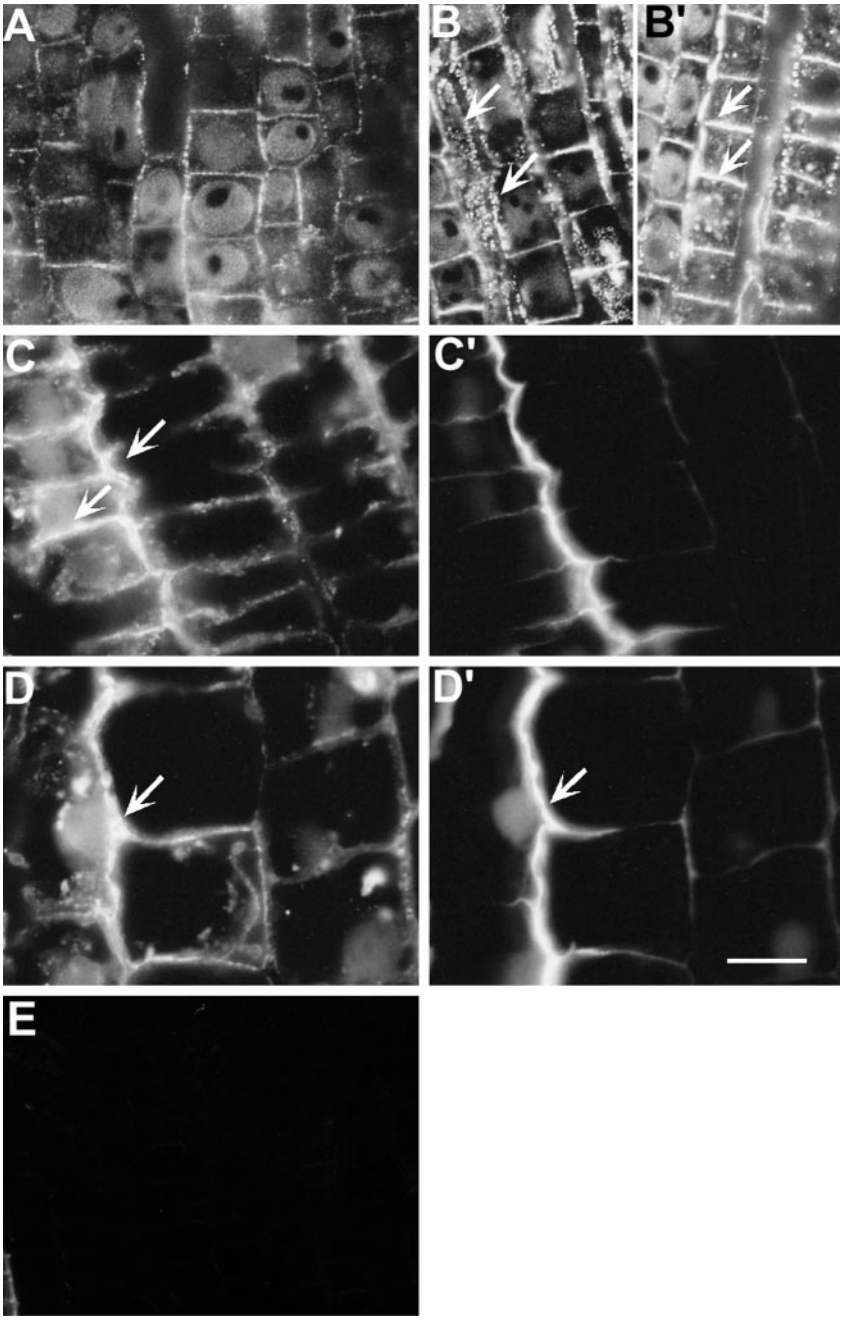

Figure 8. Effect of Al (20 μM, 3 h) on the expression of calreticulin probed with polyclonal antibody (immunofluorescence technique) and its colocalization with Al-induced callose in wheat cv Scout 66 root apex. Control image (A) is showing basal fluorescence of calreticulin preferentially lining the cortex cell pit-field peripheries as fine dots. Increased fluorescence in the same pit-field regions was apparent after Al treatments (B, B′, C, and D). Arrows in B and B′ showing cortical cells with enhanced intensity both from the longitudinal and transverse regions of cell peripheries. Similar expression was found at epidermal cells (arrows in C) and the same regions were characterized with the enhanced callose (C′). This pattern of colocalization continued all along the root apex as evidenced by the expression at the middle part of transition region epidermal cells (D) and the callose version (D′) of the same frame (arrows). Note that the callose is not appearing as fine dots since this region of section is not paradermal (see text for details). Sections labeled without the primary antibody showed no fluorescence signal (E). Representative images of at least two independent experiments comprising four to six individual root apices. Scale bar represents 18 μm.

ultramicrotome (model OM U3, Reichert, Vienna) were collected on formvar-coated Ni grids.

Residual aldehydes on sections were blocked with 0.05 M Gly in PBS, pH 7.4, and non-specific binding of proteins was avoided by applying 5% (v/v) bovine serum albumin and 5% (v/v) normal goat serum for 30 min. Subsequently, grids were washed in a solution containing 1% (v/v) bovine serum albumin and 0.1% (v/v) gelatin fish in PBS for 5 min, then incubated with the monoclonal 1→3-β-D-glucan antibody (Biosupplies, Parkville, Australia). The sections were washed five times with washing solution (see above) and incubated with the goat anti-rabbit IgG conjugated to 15-nm gold particles (British Biocell International) for 1.5 h. After extensive washing, sections were post-fixed with 3% (v/v) glutaraldehyde (15 min) and, after a further wash, stained with uranyl acetate and lead citrate. Labeled sections were analyzed with an electron microscope (model 10A, Zeiss) at 60 kV.

Immunolocalization of Calreticulin and Myosin

Standard indirect immunofluorescence procedures were followed for the localization of calreticulin and myosin (Baluška et al., 1999; Sivaguru et al., 1999a). In brief, after designated treatments, the 10-mm root apices were dissected and transferred to 5 mL of SB containing 5% dimethyl sulfoxide for 15 min at room temperature. They

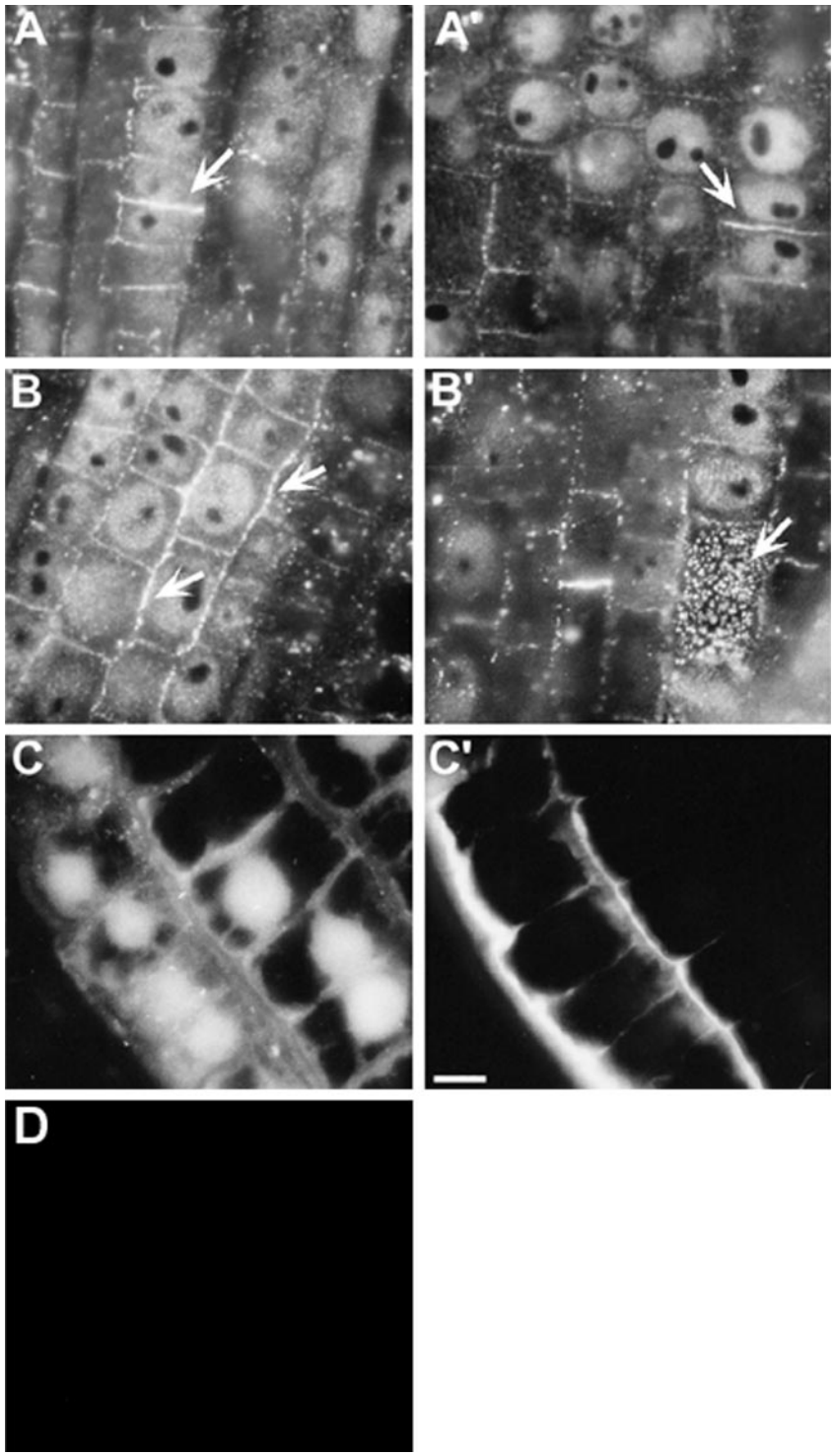

Figure 9. Effect of Al (20 μM, 3 h) on the expression of myosin VIII probed with polyclonal antibody and its colocalization with Al-induced callose in wheat cv Scout 66 root apex. Control images (A and A′) show myosin VIII fluorescence associated with inner cortex pit-fields in the form of fine dots, except bright fluorescence at callosic cell plates (arrows in A and A′). In contrast, overall brighter fluorescence is apparent after Al treatments (B, B′, and C). B (longitudinal cell walls, arrows) and B′ (paradermal section, arrow) images document the Al-induced myosin VIII accumulation at callosic pit-fields of cortex cells. The Al-induced callose deposition lining the PM of the outermost cortex cells facing the epidermis is not associated with proportional myosin VIII accumulation (compare C and C′ with Fig. 8, C and C′, for calreticulin). All images are from the 1- to 2-mm region of the root apex. Sections labeled without the primary antibody showed no fluorescence signals (D). Representative images of at least two independent experiments comprising four to six individual root apices. Scale bar represents 12 μm.

were then fixed with 4% (v/v) paraformaldehyde in SB containing 10% (v/v) dimethyl sulfoxide for 60 min at room temperature with initial 10 min under vacuum. After three 10-min rinses in PBS, to facilitate antibody penetration, they were digested with an enzymatic cocktail (1% [w/v] Hemicellulase [from *Aspergillus niger*, Sigma-Aldrich, Tokyo], 1% [w/v] Pectolyase [Seishin Corporation, Tokyo], 0.5 M EGTA, 0.4 M Mannitol, 1% [v/v] Triton X-100, and 0.3 mM phenylmethylsulfonyl fluoride, all dissolved in SB) for 60 min. The digestion reaction was terminated by transferring the roots to SB for 15 min followed by 1% (v/v) Triton X-100 in SB for 10 min. After a brief rinse in SB, the roots were extracted in HPLC grade absolute methanol at −20°C for 10 min, rehydrated in PBS (2 h), and incubated with rabbit polyclonal anticalreticulin or myosin antibodies diluted 1:200 in PBS for 12 h in dark at room

temperature. The roots were then incubated with fluorescein isothiocyanate-conjugated anti-rabbit IgG raised in goat (Sigma-Aldrich) diluted 1:100 in PBS for 12 h at room temperature. Parallel sets of roots processed without primary antibodies served as negative controls showed no fluorescence signals (data not shown). The procedure was completed by transferring the labeled roots to 0.01% (w/v) toluidine blue in PBS to diminish the autofluorescence of the tissue and mounted in Mowiol (Calbiochem-Novabiochem, La Jolla, CA).

Western blots performed with the total wheat root apex (0–2 mm) proteins (soluble fraction) showed single bands against both calreticulin and myosin VIII antibodies (data not shown).

Microinjections

After specified treatment, a single intact wheat plant was secured under an epifluorescence microscope (model BX 50 WI, Olympus, Tokyo) fitted with a blue (barrier pass 390–490) excitation filter coupled with a standard microinjection (Narishige, Tokyo) facility. The probe LYCH, obtained from Molecular Probes (Eugene, OR), was dissolved in potassium hydrogen carbonate buffer at a needle concentration of 1 mM. The roots were pre-equilibrated with 0.2 M mannitol, as this decreases slightly the turgor pressure of the cells, thereby increasing the success rate of microinjection (Cleland et al., 1994). The epidermal and cortical cells were pressure-microinjected (injection pressure, 750 hPa) in 1-s pulses (7362 Transjector Basic, Eppendorf) using Femtotips (Eppendorf, Netheler-Hinz, Hamburg, Germany), connected with a triple axial manual micromanipulator (Narishige). In the case of tobacco (*Nicotiana tabacum* L. cv Xanthi) plants, the microinjections were performed in a mature, healthy leaf of wild-type plants grown under controlled environmental conditions, mounted under the microscope in a live condition after epidermal peeling. All other conditions were identical with wheat root injections, except the injection pressure (450 hPa), and the Al treatments were performed on the microscope stage by soaking the exposed mesophyll cells with an appropriate Al solution and before injections washed thoroughly with control solution and bathed in 0.2 M mannitol. The dye fluorescence was recorded as quick as possible (seconds to minutes) in a color-chilled 3CCD camera (model 3204 C, Olympus), and the images in red-green-blue format were stored permanently in the hard disc. Where needed, injections were performed in plants using Al + LYCH mixture in both wheat and tobacco mesophyll cells pretreated with or without Al. Microinjection experiments were repeated under identical conditions for at least six to eight times under a range of Al and other treatment conditions with appropriate replicates each time.

ACKNOWLEDGMENT

Our sincere thanks are due to Dr. Tobias I. Baskin (Division of Biological Sciences, University of Missouri, Columbia) for his kind assistance with digital printing.

Received March 10, 2000; accepted July 10, 2000.

LITERATURE CITED

Baluška F, Šamaj J, Napier R, Volkmann D (1999) Maize calreticulin localizes preferentially to plasmodesmata in root apex. Plant J **19:** 481–488

Baluška F, Volkmann D, Barlow PW (2000) Actin-based domains of the "cell periphery complex" and their associations with polarized "cell bodies" in higher plants. Plant Biol **2:** 253–267

Barlow PW, Baluška F (2000) Cytoskeletal perspectives on root growth and morphogenesis. Annu Rev Plant Physiol Plant Mol Biol **51:** 289–322

Baron-Epel O, Hernandez D, Jiang L-W, Meiners S, Schindler M (1988) Dynamic continuity of cytoplasmic and membrane compartments between plant cells. J Cell Biol **106:** 715–721

Blackman LM, Harper JDI, Overall RL (1999) Localization of a centrin-like protein to higher plant plasmodesmata. Eur J Cell Biol **78:** 297–304

Blackman LM, Overall RL (1998) Immunolocalization of the cytoskeleton to plasmodesmata of *Chara corallina*. Plant J **14:** 733–741

Blancaflor EB, Jones D, Gilroy S (1998) Alterations in the cytoskeleton accompanies aluminum-induced growth inhibition and morphological changes in primary roots of maize. Plant Physiol **118:** 159–172

Boevink P, Oparka KJ, Santa Cruz S, Martin B, Betteridge A, Hawes C (1998) Stacks on tracks: the plant Golgi apparatus traffics on an actin/ER network. Plant J **15:** 441–447

Clarke SE (1996) Plant cell communication: the world outside the plasma membrane. Trends Plant Sci **1:** 406–407

Cleland RE, Fujiwara T, Lucas WJ (1994) Plasmosdesmal-mediated cell-to-cell transport in wheat roots is modulated by anaerobic stress. Protoplasma **178:** 81–85

Ding B, Kwon MO, Warnberg L (1996) Evidence that actin filaments are involved in controlling the permeability of plasmodesmata in tobacco mesophyll. Plant J **10:** 157–164

Ding B, Turgeon R, Parthasarathy MV (1992) Substructure of freeze substituted plasmodesmata. Protoplasma **169:** 28–41

Duckett CM, Oparka KJ, Prior DAM, Dolan L, Roberts K (1994) Dye coupling in the root epidermis of *Arabidopsis* is progressively reduced during development. Development **120:** 3247–3255

Epel B, Padgett HS, Heinlein M, Beachy RN (1996) Plant virus movement protein dynamics probed with a movement protein fused to GFP. Gene **173:** 75–79

Epel BL (1994) Plasmodesmata: composition, structure and trafficking. Plant Mol Biol **26:** 1343–1356

Epel BL, Erlanger MA (1991) Light regulates symplastic communication in etiolated corn seedlings. Physiol Plant **83:** 149–153

Estelle M (1998) Polar auxin transport: new support for an old model. Plant Cell **10:** 1775–1778

Fujiwara T, Giesman-Cookmeyer D, Ding B, Lommel SA, Lucas WJ (1991) Cell-to-cell trafficking of macromolecules through plasmodesmata potentiated by the red

clover necrotic mosaic virus movement protein. Plant Cell **5:** 1783–1794

Gharyal P, Ho S-C, Wang JL, Schindler M (1989) *O*-antigen from *Bradyrhizobium japonicum* lipopolysaccharide inhibits intercellular (symplast) communication between soybean (*Glycine max*) cells. J Biol Chem **264:** 12119–12121

Gisel A, Barella S, Hempel FD, Zambryski PC (1999) Temporal and spatial regulation of symplastic trafficking during development in *Arabidopsis thaliana* apices. Development **126:** 1879–1889

Gruhn P, Goletti F, Roy RN (1995) A 2020 vision for food agriculture and the environment: the vision, challenge, and recommended action. *In* P Gruhn, F Goletti, RN Roy, eds, Plant Nutrient Management, Food Security and Sustainable Agriculture: The Future Through 2020. International Food Poli Press, Washington, DC, pp 1–5

Holdaway-Clarke TL, Walker NA, Hepler PK, Overall RL (2000) Physiological elevations in cytoplasmic free calcium by cold or ion injection result in transient closure of higher plant plasmodesmata. Planta **210:** 329–335

Horst WJ (1995) The role of the apoplast in aluminum toxicity and resistance of higher plants: a review. Z Pflanzenernäehr Bodenkd **158:** 419–428

Iglesias VA, Meins F Jr (2000) Movement of plant viruses is delayed in a β-1,3-glucanase-deficient mutant showing a reduced plasmodesmatal size exclusion limit and enhanced callose deposition. Plant J **21:** 157–166

Jones DL, Gilroy S, Larsen PB, Howell SH, Kochian LV (1999) Effect of aluminum on cytoplasmic Ca^{2+} homeostasis in root hairs of *Arabidopsis thaliana* (L.). Planta **206:** 378–387

Jones DL, Kochian LV, Gilroy S (1998) Aluminum induces a decrease in cytosolic calcium concentration in BY-2 tobacco cell cultures. Plant Physiol **116:** 81–89

Kauss H (1996) Callose synthesis. *In* M Smallwood, JP Knox, DJ Bowles, eds, Membranes: Specialized Functions in Plants. BIOS Scientific Publishers, Oxford, pp 77–92

Kochian LV (1995) Cellular mechanisms of aluminum toxicity and resistance in plants. Annu Rev Plant Physiol Mol Biol **46:** 237–260

Kollmeier M, Felle HH, Horst WJ (2000) Genotypical differences in aluminum resistance of maize are expressed in the distal part of the transition zone: is reduced basipetal auxin flow involved in inhibition of root elongation by aluminum? Plant Physiol **122:** 945-956

Kragler F, Lucas WJ, Monzer J (1998) Plasmodesmata: dynamics, domains and patterning. Ann Bot **81:** 1–10

Krause KH, Michalak M (1997) Calreticulin. Cell **88:** 439–443

Larsen PB, Kochian LV, Howell SH (1997) Al inhibits both shoot development and root growth in als3, an Al-sensitive *Arabidopsis* mutant. Plant Physiol **114:** 1207–1214

Lazarowitz SG, Beachy RN (1999) Viral movement proteins as probes for intracellular and intercellular trafficking in plasmodesmata. Plant Cell **11:** 535–548

Lee J-Y, Yoo B-C, Lucas WJ (2000) Parallels between nuclear-pore and plasmodesmal trafficking of informational molecules. Planta **210:** 177–187

Lomax TC, Muday GK, Rubery PH (1995) Auxin transport. *In* PJ Davies, ed, Plant Hormones: Physiology, Biochemistry and Molecular Biology. Kluwer Academic Publishers, Dordrecht, The Netherlands, pp 509–530

Lucas WJ (1995) Plasmodesmata: intercellular channels for macromolecular transport in plants. Curr Opin Cell Biol **7:** 673–680

Lucas WJ (1999) Plasmodesmata and the cell-to-cell transport of proteins and nucleoprotein complexes. J Exp Bot **50:** 979–987

Lucas WJ, Ding B, van der Schoot C (1993) Plasmodesmata and the supracellular nature of plants. New Phytol **125:** 435–476

Lucas WJ, Gilbertson RL (1994) Plasmodesmata in relation to viral movement within leaf tissues. Annu Rev Phytopathol **32:** 387–411

Matsumoto H (2000) Cell biology of Al tolerance and toxicity in higher plants. Int Rev Cytol **200:** 1–46

Meikle PJ, Bonig I, Hoogenrad NJ, Clarke AE, Stone BA (1991) The location of (1→3)-β-glucan in the walls of pollen tubes of *Nicotiana alata* using a (1→3)-β-glucan specific monoclonal antibody. Planta **185:** 1–8

Merry L, Mesaeli N, Michalak M, Opas M, Lew DP, Krause KH (1996) Overexpression of calreticulin increases intracellular Ca^{2+} storage and decreases store-operated Ca^{2+} influx. J Biol Chem **271:** 9332–9339

Mezitt LA, Lucas WJ (1996) Plasmodesmal cell-to-cell transport of proteins and nucleic acids. Plant Mol Biol **32:** 251–273

Miller D, Hable W, Gottwald J, Ellard-Ivey M, Demura T, Lomax T, Carpita N (1997) Connections: the hard wiring of the place cell for perception, signaling and response. Plant Cell **9:** 2105–2117

Moffat AS (1999) Engineering plants to cope with metals. Science **285:** 369–370

Müller A, Guan C, Gälweiler L, Tänzler P, Huijser P, Marchant A, Parry G, Bennett M, Wisman E, Palme K (1998) AtPIN2 defines a locus of *Arabidopsis* for root gravitropism control. EMBO J **17:** 6903–6911

Oparka KJ, Prior DAM (1992) Direct evidence for pressure generated closure of PD. Plant J **2:** 741–750

Oparka KJ, Roberts AG, Boevink P, Santa Cruz S, Roberts I, Pradel KS, Imlau A, Kotlitzky G, Sauer N, Epel B (1999) Simple, but not branched, plasmodesmata allow the nonspecific trafficking of proteins in developing tobacco leaves. Cell **97:** 743–754

Overall RL, Blackman LM (1996) A model of the macromolecular structure of plasmodesmata. Trends Plant Sci **1:** 307–311

Radford JE, Vesk M, Overall RL (1998) Callose deposition at plasmodesmata. Protoplasma **201:** 30–37

Radford JE, White RG (1998) Localization of a myosin-like protein to plasmodesmata. Plant J **14:** 743–750

Rashotte AM, Brady SR, Reed RC, Ante SJ, Muday GK (2000) Basipetal auxin transport is required for gravitropism in roots of *Arabidopsis*. Plant Physiol **122:** 481–490

Reichelt S, Knight AE, Hodge TP, Baluška F, Šamaj J, Volkmann D, Kendrick-Jones J (1999) Characterization of the unconventional myosin VIII in plant cells and its

localization at the post-cytokinetic cell wall. Plant J **19:** 555–569

Rengel Z (1996) Uptake of aluminum by plant cells. New Phytol **134:** 389–406

Robards AW, Lucas WJ (1990) Plasmodesmata. Annu Rev Plant Physiol Plant Mol Biol **41:** 369–419

Rodriguez-Gálvez E, Mendgen K (1995) Cell wall synthesis in cotton roots after infection with *Fusarium oxysporum*: the deposition of callose, arabinogalactans, xyloglucans, and pectic components into walls, wall apositions, cell plates and plasmodesmata. Planta **197:** 535–545

Sanderson MJ (1995) Intercellular calcium waves mediated by inositol triphosphate-calcium waves, gradients and oscillations. Ciba Found Symp **188:** 175–194

Seju K, Lee Y (1998) Aluminum induces changes in the orientation of microtubules and the division plane in root meristem of *Zea mays*. J Plant Biol **41:** 269–276

Silva IR, Smyth TJ, Moxley DF, Carter TE, Allen NS, Rufty TW (2000) Aluminum accumulation at nuclei of cells in the root tip: fluorescence detection using lumogallion and confocal laser scanning microscopy. Plant Physiol **123:** 543–552

Sivaguru M, Baluška F, Volkmann D, Felle HH, Horst WJ (1999a) Impacts of aluminum on the cytoskeleton of the maize root apex: short-term effects on the distal part of the transition zone. Plant Physiol **119:** 1073–1082

Sivaguru M, Horst WJ (1998) The distal part of the transition zone is the most aluminum-sensitive apical root zone of maize. Plant Physiol **116:** 155–163

Sivaguru M, Yamamoto Y, Matsumoto H (1999b) Differential impacts of aluminum on microtubule organization depends on growth phase in suspension-cultured tobacco cells. Physiol Plant **107:** 110–119

Taylor GJ (1995) Overcoming barriers to understanding the cellular basis of aluminum resistance. Plant Soil **171:** 89–103

Tucker EB (1988) Inositol bisphosphate and inositol trisphosphate inhibit cell-to-cell passage of carboxyfluorescein in staminal hair cells of *Setcreasea purpurea*. Planta **174:** 358–363

Tucker EB (1990) Calcium loaded 1,2-bis (2-aminophenoxy) ethane-*N N*, *N*′, *N*′-tetra acetic acid blocks cell-cell diffusion of carboxyfluorescein in staminal hairs of *Setcreasea purpurea*. Planta **182:** 34–38

Tucker EB, Boss WF (1996) Mastoparan-induced Ca^{2+} fluxes regulate cell-cell communication. Plant Physiol **111:** 459–467

Van Bel AJE, Oparka KJ (1995) On the validity of plasmodesmograms. Bot Acta **108:** 174–182

White RG, Badett K, Overall RL, Vesk M (1994) Actin associated with plasmodesmata. Protoplasma **180:** 169–184

Wolf S, Deom CM, Beachy RN, Lucas WJ (1989) Movement protein of tobacco mosaic virus modifies plasmodesmatal size exclusion limit. Science **246:** 377–379

Wyatt SE, Carpita NC (1993) The plant cytoskeleton-cell-wall continuum. Trends Cell Biol **3:** 413–417

Xhu T, Lucas WJ, Rost TL (1998) Directional cell-to-cell communication in the *Arabidopsis* root apical meristem: I. An ultrastructural and functional analysis. Protoplasma **203:** 35–47

Yahalom A, Lando R, Katz A, Epel BL (1998) A calcium-dependent protein kinase is associated with maize mesocotyl plasmodesmata. J Plant Physiol **153:** 354–362

Zambryski P (1995) Plasmodesmata: plant channels for molecules on the move. Science **270:** 1943–1944

Zhang G, Hoddinott J, Taylor GJ (1994) Characterization of 1→3-β-glucan (callose) synthesis in roots of *Triticum aestivum* in response to aluminum toxicity. J Plant Physiol **144:** 229–234

Zhang W-H, Rengel Z (1999) Aluminum induces an increase in cytoplasmic calcium in intact wheat root apical cells. Aust J Plant Physiol **26:** 401–409